Improved charge balance in green perovskite light-emitting diodes with atomic layer-deposited Al_2O_3

William B. Gunnarsson[a], Zhaojian Xu[a], Nakita K. Noel[a,b], Barry P. Rand[a,c] *

[a] Department of Electrical and Computer Engineering, Princeton University, Princeton, NJ 08544, USA

[b] Princeton Institute for the Science and Technology of Materials, Princeton University, Princeton, NJ 08544, USA

[c] Andlinger Center for Energy and the Environment, Princeton University, Princeton, NJ 08544, USA

* Corresponding author, email: brand@princeton.edu

Keywords: metal halide perovskite, LED, charge balance, $CsPbBr_3$, ZnO, Al_2O_3, atomic layer deposition

Abstract:

Perovskite light-emitting diodes (LEDs) have experienced a rapid increase in efficiency over the last several years and are now regarded as promising low-cost devices for displays and communication systems. However, it is often challenging to employ ZnO, a well-studied electron transport material, in perovskite LEDs due to chemical instability at the ZnO/perovskite interface and charge injection imbalance caused by the relatively high conductivity of ZnO. In this work, we address these problems by depositing an ultrathin Al_2O_3 interlayer at the ZnO/perovskite interface, allowing the fabrication of green-emitting perovskite LEDs with a maximum luminance of 21,815 cd/m^2. Using atomic layer deposition, we can precisely control the Al_2O_3 thickness and thus fine-tune the electron injection from ZnO, allowing us to enhance the efficiency and operational stability of our LEDs.

INTRODUCTION

Metal halide perovskites are promising candidates for next-generation low-cost light-emitting diodes (LEDs), owing to their impressive photoluminescence quantum efficiency, tunable emission wavelength, and high color purity[1–5]. However, the development of perovskite devices is frequently hindered by the chemical and thermal instability of perovskite films, particularly those containing ammonium-based organic molecules[6–9]. One such source of instability is the interface between the perovskite emissive layer (EmL) and ZnO, an electron transport material commonly used in non-perovskite electronic and optoelectronic devices due to its superior optical transparency, high electron mobility, and ease of fabrication[10]. At this interface, the alkaline ZnO surface can deprotonate ammonium-containing molecules in the perovskite, as well as the more chemically stable alternative, formamidinium, leading many researchers to abandon ZnO or change perovskite composition[11–13].

Furthermore, several reports have noted that the use of ZnO electron transport layers (ETLs) in LEDs can lead to unbalanced injection of electrons and holes into the EmL due to mismatched conductivities of ZnO and commonly used organic hole transport layers (HTLs)[14–17]. Such an imbalance can lead to unwanted buildup of electrons at the EmL/HTL interface, which can severely compromise the efficiency and operational stability of the device[18,19]. One possible solution is to dope the ZnO layer with a metal such as cobalt[14], yttrium[15], or magnesium[16] to lower the concentration and mobility of electrons in the ETL, and thereby reduce electron injection into the EmL. A different strategy, employed by Dai, et al., is to insert a thin layer of an insulating polymer between the EmL and the ZnO ETL to restrict electron transfer and create balanced charge injection[17].

In this work, we address both the instability of the ZnO/perovskite interface and the imbalanced injection of electrons and holes by applying an ultrathin layer of Al_2O_3 deposited by atomic layer deposition (ALD) between the ZnO ETL and perovskite EmL. We show that an interposed polymer layer is insufficient to prevent the reaction between the ZnO surface and ammonium-containing perovskite additives, but just a fraction of a nanometer of Al_2O_3 completely inhibits the reaction. Moreover, ALD affords precise control

of the Al_2O_3 layer thickness, which enables careful tuning of electron injection mediated by tunneling through the Al_2O_3. By inserting an optimized Al_2O_3 layer, we demonstrate enhanced maximum luminance from 82 cd/m^2 to 21,815 cd/m^2, with similar improvements to efficiency and operational stability.

RESULTS AND DISCUSSION

We use $(PEABr)_{0.4}CsPbBr_3$ (where PEABr = phenylethylammonium bromide) as our perovskite emissive layer, where PEABr is included to enhance the luminescence and morphology of the film. Our ETL stack consists of sequentially deposited ZnO, Al_2O_3, and polyethylenimine ethoxylated (PEIE). The thin PEIE interfacial layer is added to improve the energy alignment of the ZnO/Al_2O_3 and perovskite, which allows Ohmic electron injection into the perovskite. When deposited on glass/PEIE substrates (i.e. no ZnO or Al_2O_3 is included), our $(PEABr)_{0.4}CsPbBr_3$ films exhibit bright steady-state photoluminescence (ssPL) with a peak wavelength of 513 nm, as shown in Figure 1a. However, when the perovskite is deposited on our ETL stack with 0 cycles of ALD Al_2O_3, we observe severe luminescence quenching stemming from the ZnO/perovskite interface, accompanied by a small (~5 nm) redshift which will be discussed below. Notably, the observed quenching is nearly independent of the PEIE thickness, even when deposited from a solution with 0.2% PEIE by weight, corresponding to a thickness of approximately 5 nm (see Figure S1). We characterized the PEIE films by X-ray photoelectron spectroscopy (XPS) and atomic force microscopy (AFM), shown in Figure S2, to ensure complete coverage and survival of the PEIE films during perovskite deposition. With the addition of 2, 8, or 20 cycles of ALD Al_2O_3 on the ZnO surface, the ssPL response of the perovskite is fully restored. Similarly, time-resolved PL (trPL) measurements, shown in Figure 1b, reveal a 3-fold reduction in PL lifetime when the perovskite film is deposited on the ETL stack with 0 cycles of ALD Al_2O_3, compared to the sample with no ETL. The addition of ALD Al_2O_3 on the ZnO surface enhances the PL lifetime to nearly match that of the sample with no ETL, with a slight improvement observed for thicker Al_2O_3 layers. In both ssPL and trPL measurements, just 2 cycles of ALD Al_2O_3 is sufficient to mitigate the quenching effect of the perovskite/ZnO interface. Each ALD Al_2O_3 cycle

yields 0.12 nm of Al_2O_3, characterized by ellipsometry as shown in Figure S3, though nucleation of the film is likely incomplete after only 2 cycles. Therefore, the 2-cycle Al_2O_3 film is not capable of forming a complete physical barrier between the ZnO and perovskite, but must instead chemically passivate the reactive sites on the ZnO surface.

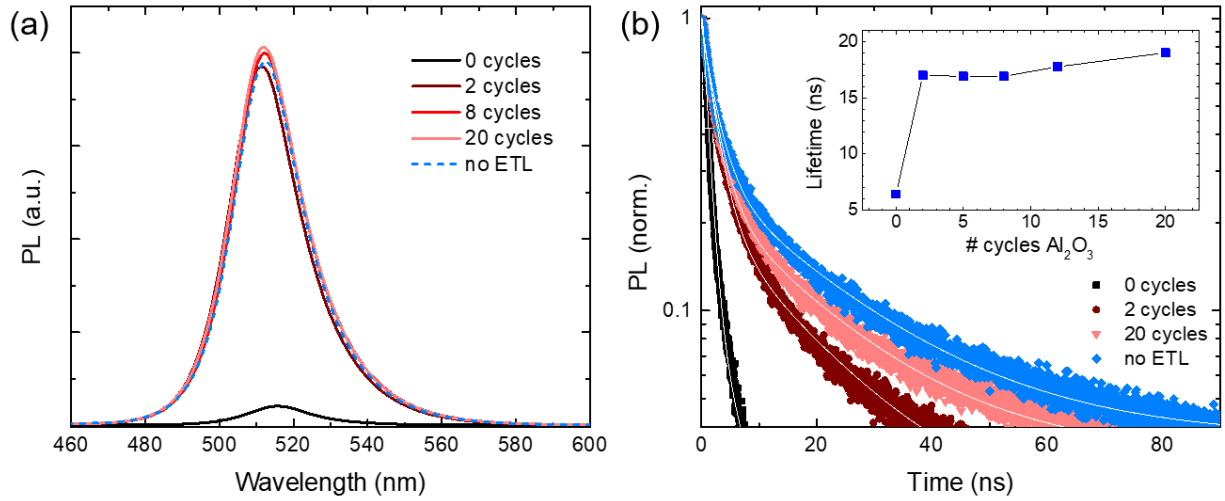

Figure 1: (a) Steady-state and (b) time-resolved PL response of perovskite films deposited on ZnO/Al_2O_3/PEIE ETL stacks, with varied number of ALD Al_2O_3 cycles. Photoluminescence lifetimes were extracted using biexponential fits, shown as white lines in (b). The inset shows PL lifetime vs. number of ALD Al_2O_3 cycles. Samples labeled "no ETL" have the structure glass/PEIE/perovskite.

Using XPS, we confirmed the presence of a reaction between the ZnO surface and the ammonium group in our perovskite additive, PEABr. This reaction has previously been reported at the interface of ZnO and $MAPbI_3$ perovskite, where the methylammonium (MA^+) cation is deprotonated by the alkaline ZnO surface, and has largely impeded the use of ZnO transport layers in $MAPbI_3$ solar cells and LEDs[12,13]. We observed the *N 1s* XPS signal from a very thin (< 10 nm) film of $(PEABr)_{0.4}CsPbBr_3$ on ZnO, with and without an interlayer of 2 cycles of Al_2O_3 (PEIE was not included in these samples, as its nitrogen component would obscure the *N 1s* signal from the perovskite). As shown in Figure 2a, the sample without an Al_2O_3 interlayer displays two *N 1s* peaks at 402.4 and 400.5 eV, corresponding to pristine and deprotonated PEABr, respectively[20]. The sample with an Al_2O_3 interlayer shows no evidence of deprotonated PEABr, with a single peak at 402.4 eV in the *N 1s* spectrum.

Absorption measurements, shown in Figure 2b, were performed on glass/ZnO/Al_2O_3/PEIE/$(PEABr)_{0.4}CsPbBr_3$ film stacks to further elucidate the impact of the proton-transfer reaction on the optical properties of the perovskite films. Owing to the quasi-2D nature of $(PEABr)_{0.4}CsPbBr_3$ perovskite, the absorption spectrum of the sample with no ETL contains excitonic features at 404, 435, 466, and 482 nm, which result from layered perovskite structures with n = 1, 2, 3, and 4, respectively[21,22]. While the samples with 2 or more cycles of ALD Al_2O_3 deposited on the ZnO surface yield absorption spectra identical to that of the sample with no ETL, the sample with 0 cycles of Al_2O_3 shows no quasi-2D excitonic features, and instead produces an absorption spectrum characteristic of a 3D $CsPbBr_3$ film. This is consistent with the loss of PEABr due to the proton-transfer reaction observed in XPS, and further indicates that the PEIE layer beneath the perovskite is unable to prevent the reaction between ZnO and $(PEABr)_{0.4}CsPbBr_3$. These results were corroborated by X-ray diffraction (XRD) measurements, shown in Figure S4. The redshift in the ssPL spectrum (Figure 1a) of the ZnO/PEIE/perovskite sample can also be attributed to the deprotonation of PEABr and consequent destruction of the quasi-2D structure, as the confinement of charge carriers in the quasi-2D quantum wells leads to larger exciton binding energy and thus higher-energy luminescence.

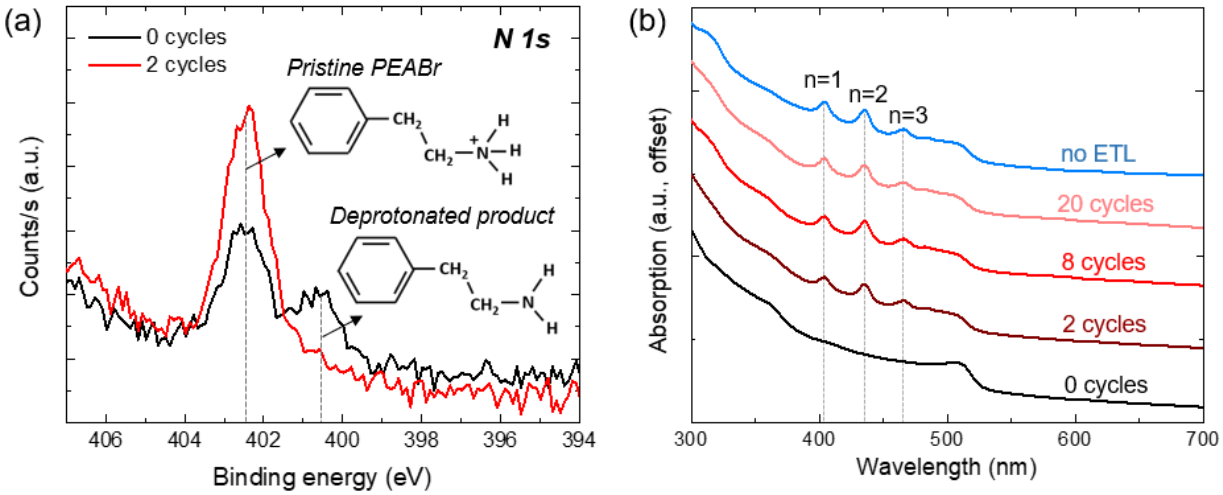

Figure 2: (a) XPS *N 1s* spectra of thin (< 10 nm) perovskite films deposited on ZnO with or without an Al_2O_3 interlayer of 2 ALD cycles. Dashed lines indicate the photoelectron signals from pristine and deprotonated PEABr, and the molecular structures of both are shown. (b) Absorption spectra of perovskite films deposited on ZnO/Al_2O_3/PEIE ETL stacks, with varied number of ALD Al_2O_3 cycles. Excitonic

absorption peaks from layered perovskite regions with n = 1, 2, and 3 are indicated with dashed lines. The sample labeled "no ETL" has the structure glass/PEIE/perovskite.

We fabricated perovskite LEDs with the following device structure: ITO/ZnO/Al_2O_3/PEIE/perovskite/polyTPD/MoO_3/Au, where polyTPD = poly[*N*,*N*'-bis(4-butylphenyl)-*N*,*N*'-bis(phenyl)-benzidine]. The energy band diagram for this structure is shown in Figure 3a. The electroluminescence (EL) spectrum exhibits a slight narrowing and redshift relative to the PL (see Figure 3b), resulting from the quasi-2D structure of the perovskite, which funnels carriers into regions of large n and thus smaller bandgap. This effect is slightly more pronounced in the EL spectrum, as electrically injected carriers are less likely to form excitons in the low-n, large-bandgap regions, though excitons can be photogenerated in low-n regions in the case of PL. Figure 3c shows the performance of perovskite LEDs with varied Al_2O_3 thickness as the device bias is swept from 0 to 6 V. The Al_2O_3 thickness has a pronounced effect on the current density-voltage (*J-V*) characteristics; in particular, the turn-on voltage increases by 0.3 - 0.5 V with each additional 4 ALD cycles of Al_2O_3 due to the tunneling-mediated restriction of electron current. Notably, the Al_2O_3 layer has no significant effect on the series resistance of the LED when fewer than 20 cycles are deposited. A slight increase in series resistance can be seen for the device with 20 cycles Al_2O_3. The *J-V* relations are shown on a linear scale in Figure S5 to highlight the relative series resistance of each device.

The addition of the Al_2O_3 layer greatly enhances LED performance, though this requires a much thicker layer than the 2 cycles needed for surface passivation. Without an Al_2O_3 layer, our perovskite LED structure displays reasonable *J-V* characteristics, but reaches a maximum luminance of just 82 cd/m^2 and EQE of 0.005% (see "0 cycles" in Figures. 3c and 3d). With an optimized Al_2O_3 layer of 16 ALD cycles, we observe bright electroluminescence with a peak luminance of 21,815 cd/m^2 and external quantum efficiency (EQE) of 2.7%. We note that the maximum EQE is limited by the low photoluminescence quantum efficiency (PLQE) of the perovskite film (see Figure S6). Both luminance and EQE exhibit strong dependence on Al_2O_3 thickness, improving 3-fold as the thickness increases from 8 to 16 cycles.

Additionally, the EL turn-on occurs at progressively lower current density for LEDs with thicker Al_2O_3 layers (10, 4, and 2 mA/cm^2 for 8, 12, and 16 cycles Al_2O_3, respectively, determined by the change of slope in Figure 3d), indicating that the density of traps in the recombination zone decreases as Al_2O_3 thickness increases. Figure S7 shows statistics taken from several identical devices for each Al_2O_3 thickness.

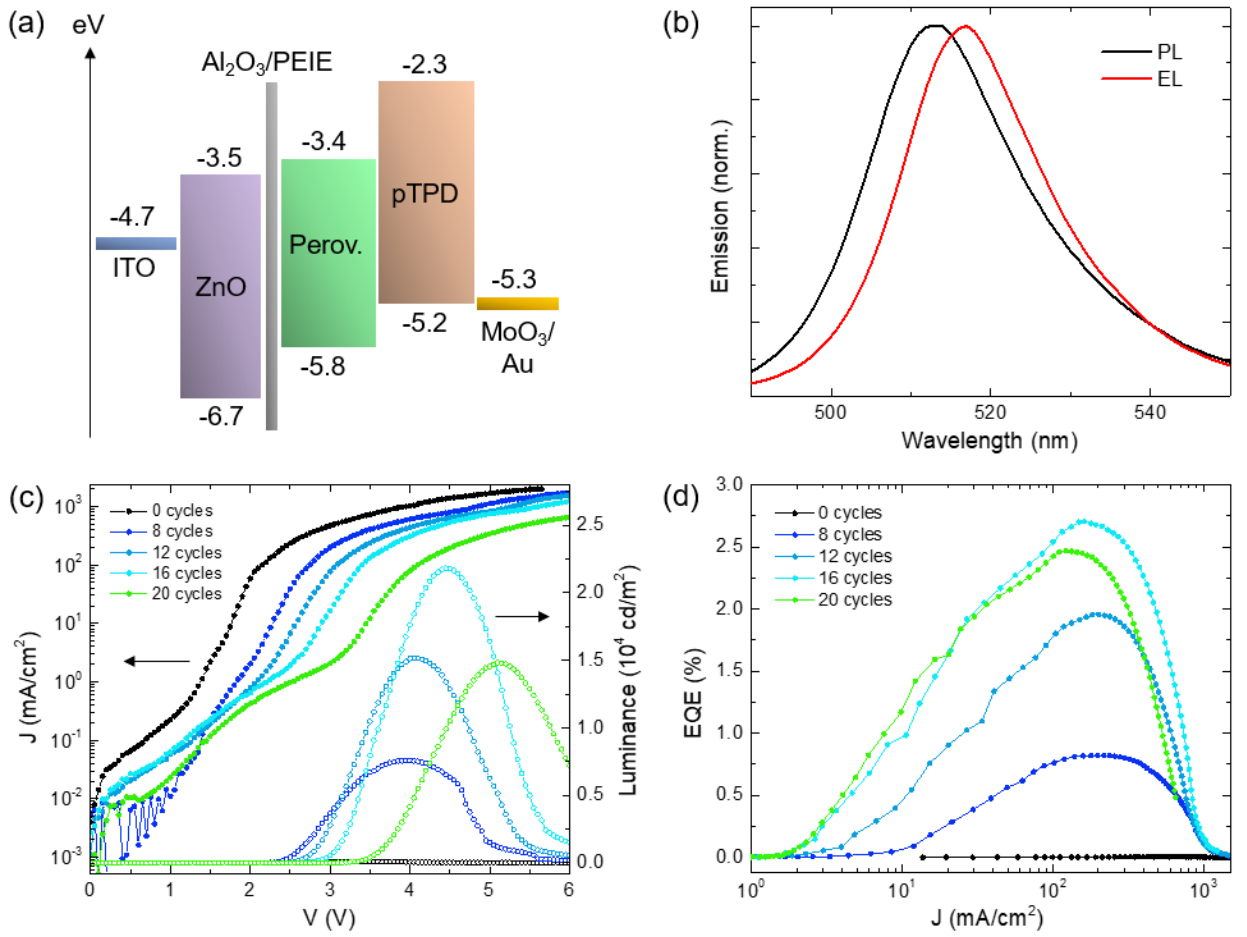

Figure 3: (a) Energy band diagram for the LED structure. (b) Normalized EL and PL spectra collected from a perovskite LED ($J \approx 100$ mA/cm^2) and a perovskite film on glass, respectively. (c) Current density (J) and luminance for LEDs with varied Al_2O_3 thickness as the applied bias (V) is swept from 0 to 6 V. (d) EQE vs. J of LEDs with varied Al_2O_3 thickness.

The LEDs also benefit from improved operational stability when the optimized Al_2O_3 layer is included. Figure 4a shows the normalized emission intensity from LEDs with varied Al_2O_3 thickness as the devices are held at a constant current density of 10 mA/cm^2. Note that the emission from LEDs with no Al_2O_3 is too weak to be measured at 10 mA/cm^2, so these were not included in the stability comparison.

Measured values of T_{80} were 41, 137, 376, and 134 s for 8, 12, 16, and 20 cycles of Al_2O_3, respectively, which closely resembles the trend in peak luminance vs. number of cycles Al_2O_3.

In order to explain the observed improvements in luminance, EQE, and operational stability, we propose that the Al_2O_3 layer facilitates balanced injection of electrons and holes by restricting electron injection. We assessed the impact of the Al_2O_3 layer on the carrier injection balance in our LEDs by fabricating single-carrier devices, which allow us to independently observe the rates of electron and hole injection. From Figure 4b we can see that the current density in the electron-only device (EOD) with no Al_2O_3 is 100 times greater than that in the hole-only device (HOD), indicating that our full LED with no Al_2O_3 will have a disproportionately large rate of electron injection. Note that the EOD with no Al_2O_3 shows substantial leakage current, particularly evident in the range 0 - 0.3 V. This is consistent with degradation of the perovskite film caused by the reaction and elimination of PEABr, which likely creates pinholes in the perovskite layer. At higher voltages, the *J-V* curve takes on a monoexponential shape corresponding to injection of electrons over a potential barrier. The EOD with 5 cycles of ALD Al_2O_3 exhibits a current density nearly 50 times lower than that of the 0-cycle EOD, resulting from a reduction of leakage current through the perovskite layer and partial obstruction of electron injection due to the insulating nature of Al_2O_3. For EODs with 10 or more cycles of Al_2O_3, the *J-V* relations take on a distinctly different shape, displaying a sharp slope increase at the onset of electron tunneling through the Al_2O_3 layer. The threshold voltage at which tunneling becomes significant depends linearly on the Al_2O_3 thickness and can be tuned from 2 to 3.5 V by varying the Al2O3 thickness between 10 and 20 cycles.

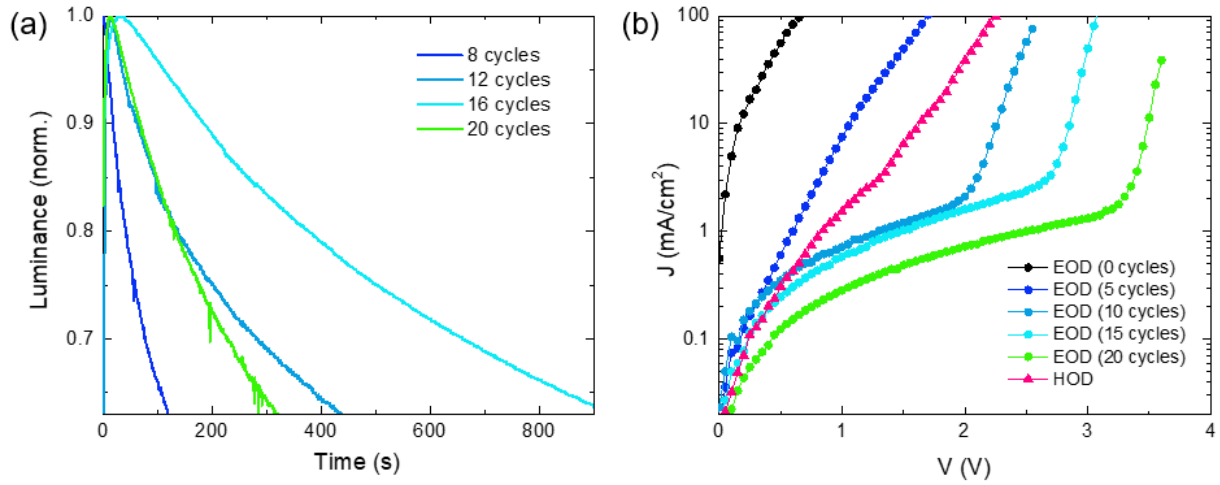

Figure 4: (a) Operational stability of LEDs with varied Al_2O_3 thickness under $J = 10$ mA/cm^2. Data for the LED with no Al_2O_3 is not included because it was not sufficiently emissive. (b) *J-V* relations of electron- and hole-only devices (EODs and HODs, respectively). The thickness of the Al_2O_3 interlayer for each EOD is indicated in the legend.

While previous studies have found that charge balance is optimized when the *J-V* curves of the EOD and HOD are similar[18,23], we see a significant disparity between the *J-V* relations of the HOD and the EOD with optimized Al_2O_3 layer (15 cycles). For instance, to reach 10 mA/cm^2, our optimized EOD requires 2.85 V applied bias whereas the HOD requires 1.65 V. This suggests that when driving our optimized LED at 10 mA/cm^2, we have a substantially larger voltage drop across the cathode/ETL layers than across the anode/HTL. Consequently, we expect the recombination zone to be shifted toward the perovskite/ETL interface. We speculate that carriers may have a greater probability of recombining radiatively here than at the perovskite/HTL interface, due to e.g. damage to the perovskite surface during solution processing of the HTL. By reducing non-radiative recombination in the EmL, we enhance both the efficiency and operational stability of our device.

When the Al_2O_3 thickness is increased to 20 cycles, the voltage drop over the Al_2O_3 during LED operation becomes prohibitively large, resulting in reduced emission and operational stability. Additionally, the onset of EQE roll-off occurs at a current density 200 mA/cm^2 lower than for devices with thinner Al_2O_3

layers (see Figure 3d). These effects are likely attributed to a combination of excessively restricted electron current and Joule heating of the Al_2O_3 layer.

CONCLUSION

In conclusion, we have demonstrated that ALD Al_2O_3 can be a valuable tool in designing perovskite LED structures. We investigated a proton-transfer reaction that occurs in a common perovskite additive at the perovskite/ZnO interface, and showed that an ultrathin Al_2O_3 interlayer can improve the chemical stability of this interface, even when a much thicker polymer interlayer fails to do so. Furthermore, ALD affords precise control of the Al_2O_3 layer thickness, allowing us to fine-tune the electron injection into the perovskite layer and improve charge balance in our LEDs. By optimizing the thickness of the Al_2O_3 interlayer, we achieved substantial improvements to luminance, EQE, and operational stability. This work provides a useful strategy for incorporating ZnO in perovskite devices with ammonium-based molecules and precisely optimizing charge balance in perovskite LEDs.

Methods:

Materials: CsBr (99.999%), phenylethylammonium bromide (PEABr, 98+%), polyethylenimine 80% ethoxylated (PEIE, 37% by weight in water), and dimethyl sulfoxide (DMSO, anhydrous, 99.9%) were purchased from Sigma Aldrich. $PbBr_2$ (98+%) and MoO_3 (99.9995%) were purchased from Alfa Aesar. PolyTPD was purchased from American Dye Source. All materials were used as received.

Device Fabrication: The perovskite precursor solution was prepared in a N_2-filled glovebox by dissolving CsBr, $PbBr_2$, and PEABr in DMSO with concentrations of 0.3 M, 0.3 M, and 0.12 M, respectively, to obtain 0.3 M $(PEABr)_{0.4}CsPbBr_3$. The precursor solution was stirred at room temperature until dissolved (~30 min), and then allowed to sit for at least 1 h before use to allow any particulates to settle. LEDs and single-carrier devices were fabricated using prepatterned ITO-coated glass substrates purchased from Colorado

Concept Coatings, with sheet resistance of 15 Ω/sq. Substrates were cleaned by sonication in Extran solution (~10% Extran in water), deionized water, acetone, and isopropyl alcohol, and then treated with O_2 plasma for 10 min. ZnO (50 cycles of diethylzinc (DEZ) and water) and Al_2O_3 (0-20 cycles of trimethylaluminum (TMA) and water) were then deposited in a Gemstar XT Thermal Atomic Layer Deposition system (Arradiance), with a substrate temperature of 125 °C. During the ZnO ALD process, DEZ and H_2O were pulsed for 35 ms, followed by a 1 s soak and 30/40 s purge for DEZ/H_2O. For Al_2O_3, TMA and H_2O were pulsed for 24 ms, followed by a 1 s soak and 30/40 s purge for TMA/H_2O. The substrates were allowed to cool before further deposition steps. PEIE (0.1 wt% in IPA) was then spin-coated at 3000 rpm for 45 s, followed by a 1 min anneal at 100 °C and 15 s low-power O_2 plasma treatment to improve wetting. The samples were then transferred to a N_2-filled glovebox for deposition of perovskite and polyTPD. The perovskite layer was spin-coated at 1000 rpm for 10 s, then 6000 rpm for 50 s (4000 rpm for single-carrier devices to reduce pinholes) and annealed at 100 °C for 2 min. PolyTPD (6 mg/ml in chlorobenzene) was then spin-coated at 6000 rpm for 45 s, followed by a 5 min, 100 °C anneal. MoO_3 (10 nm) and Au (100 nm) were thermally evaporated to complete the LEDs. The device area is 0.1 cm^2, defined by the overlap of the ITO and Au electrodes. Electron-only devices were fabricated with the structure ITO/ZnO/Al_2O_3/PEIE/perovskite/PEIE/Al_2O_3/ZnO/Ag, and hole-only devices with the structure ITO/perovskite/polyTPD/MoO_3/Au. All layers in the single-carrier devices were deposited as described above, except that Al_2O_3 and ZnO on top of the perovskite were deposited at 75 °C to minimize thermal damage to the perovskite layer. The Al_2O_3 (5 cycles) was necessary to initiate nucleation of the subsequently deposited ZnO layer. Samples for ssPL, trPL, absorption measurements, and XRD were fabricated with the structure glass/ZnO/Al_2O_3/PEIE/perovskite, with the same procedures for substrate cleaning and layer deposition as above. For PLQE measurement, $(PEABr)_{0.4}CsPbBr_3$ was deposited directly on a quartz substrate. Samples for XPS took the structure glass/ITO/ZnO/Al_2O_3/perovskite, where the perovskite solution was diluted to 0.06 M to reduce the layer thickness and allow collection of photoelectrons from the ZnO/perovskite interface.

Characterization: LEDs and single-carrier devices were measured in a N_2-filled glovebox using a custom-built setup consisting of a Keithley 2400 sourcemeter, a calibrated Si photodiode (FDS-100-CAL, ThorLabs) with a picoammeter (4140B, Agilent), and a calibrated fiber optic spectrophotometer (UVN-SR, StellarNet Inc.). The Si photodiode and the spectrophotometer fiber are attached to a motorized goniometer, which allows collection of emitted light at any angle to the normal. Steady-state and time-resolved photoluminescence were measured using an FLS980 Photoluminescence Spectrometer (Edinburgh Instruments) with 375-nm excitation. XPS analysis was performed using a Thermo Scientific K-Alpha XPS System, and absorption measurements were collected using a Cary 5000 UV-Vis-NIR Spectrometer (Agilent). XRD was measured using a Bruker D8 Discover X-ray Diffractometer. The growth rate of Al_2O_3 was measured using a Woollam M-2000 Ellipsometer. PLQE was measured using 404 nm excitation with varied intensity, and emission was collected using an integrating sphere and Spectra Pro HRS-3000 spectrometer with a PIXIS 400B CCD detector (Princeton Instruments). The surface morphology of ZnO and PEIE was characterized using a Veeco Dimension 3100 atomic force microscope.

Supporting information: additional photoluminescence measurements, XPS and AFM of PEIE films, Al_2O_3 growth rate characterization, X-ray diffraction measurements, *J-V* curves shown in linear scale, LED statistics.

Acknowledgments:

We thank Jordan Dull for assistance with ellipsometry measurements. We acknowledge support for this work from DARPA Award no. N66001-20-1-4052. W.B.G. acknowledges support by the National Science Foundation Graduate Research Fellowship Program under grant no. DGE-1656466. The authors acknowledge the use of Princeton's Imaging and Analysis Center, which is partially supported through the Princeton Center for Complex Materials (PCCM), a National Science Foundation MRSEC program (DMR-2011750).

Conflict of interest:

The authors declare no competing financial interest.

References:

(1) Quan, L. N.; Rand, B. P.; Friend, R. H.; Mhaisalkar, S. G.; Lee, T. W.; Sargent, E. H. Perovskites for Next-Generation Optical Sources. *Chem. Rev.* **2019**, *119* (12), 7444–7477. https://doi.org/10.1021/acs.chemrev.9b00107.

(2) Lu, M.; Zhang, Y.; Wang, S.; Guo, J.; Yu, W. W.; Rogach, A. L. Metal Halide Perovskite Light-Emitting Devices: Promising Technology for Next-Generation Displays. *Adv. Funct. Mater.* **2019**, *29* (30), 1902008. https://doi.org/10.1002/adfm.201902008.

(3) Quan, L. N.; García de Arquer, F. P.; Sabatini, R. P.; Sargent, E. H. Perovskites for Light Emission. *Adv. Mater.* **2018**, *30* (45), 1801996. https://doi.org/10.1002/adma.201801996.

(4) Zou, C.; Liu, Y.; Ginger, D. S.; Lin, L. Y. Suppressing Efficiency Roll-Off at High Current Densities for Ultra-Bright Green Perovskite Light-Emitting Diodes. *ACS Nano* **2020**, *14* (5), 6076–6086. https://doi.org/10.1021/acsnano.0c01817.

(5) Lin, K.; Xing, J.; Quan, L. N.; de Arquer, F. P. G.; Gong, X.; Lu, J.; Xie, L.; Zhao, W.; Zhang, D.; Yan, C.; Li, W.; Liu, X.; Lu, Y.; Kirman, J.; Sargent, E. H.; Xiong, Q.; Wei, Z. Perovskite Light-Emitting Diodes with External Quantum Efficiency Exceeding 20 per Cent. *Nature* **2018**, *562*, 245–248. https://doi.org/10.1038/s41586-018-0575-3.

(6) Prakasam, V.; Tordera, D.; Bolink, H. J.; Gelinck, G. Degradation Mechanisms in Organic Lead Halide Perovskite Light-Emitting Diodes. *Adv. Opt. Mater.* **2019**, *7* (22), 1900902. https://doi.org/10.1002/adom.201900902.

(7) Warby, J. H.; Wenger, B.; Ramadan, A. J.; Oliver, R. D. J.; Sansom, H. C.; Marshall, A. R.; Snaith, H. J. Revealing Factors Influencing the Operational Stability of Perovskite Light-Emitting Diodes. *ACS Nano* **2020**, *14* (7), 8855–8865. https://doi.org/10.1021/acsnano.0c03516.

(8) Kerner, R. A.; Rand, B. P. Electrochemical and Thermal Etching of Indium Tin Oxide by Solid-State Hybrid Organic-Inorganic Perovskites. *ACS Appl. Energy Mater.* **2019**, *2* (8), 6097–6101. https://doi.org/10.1021/acsaem.9b01356.

(9) Juarez-Perez, E. J.; Ono, L. K.; Maeda, M.; Jiang, Y.; Hawash, Z.; Qi, Y. Photodecomposition and Thermal Decomposition in Methylammonium Halide Lead Perovskites and Inferred Design Principles to Increase Photovoltaic Device Stability. *J. Mater. Chem. A* **2018**, *6* (20), 9604–9612. https://doi.org/10.1039/c8ta03501f.

(10) Zeng, J.; Qi, Y.; Liu, Y.; Chen, D.; Ye, Z.; Jin, Y. ZnO-Based Electron-Transporting Layers for Perovskite Light-Emitting Diodes : Controlling the Interfacial Reactions. *J. Phys. Chem. Lett.* **2022**, *13*, 694–703. https://doi.org/10.1021/acs.jpclett.1c04117.

(11) Kuang, C.; Hu, Z.; Yuan, Z.; Wen, K.; Qing, J.; Kobera, L.; Abbrent, S.; Brus, J.; Yin, C.; Wang, H.; Xu, W.; Wang, J.; Bai, S.; Gao, F. Critical Role of Additive-Induced Molecular Interaction on the Operational Stability of Perovskite Light-Emitting Diodes. *Joule* **2021**, *5* (3), 618–630. https://doi.org/10.1016/j.joule.2021.01.003.

(12) Yang, J.; Siempelkamp, B. D.; Mosconi, E.; De Angelis, F.; Kelly, T. L. Origin of the Thermal Instability in CH3NH3PbI3 Thin Films Deposited on ZnO. *Chem. Mater.* **2015**, *27* (12), 4229–4236. https://doi.org/10.1021/acs.chemmater.5b01598.

(13) Schutt, K.; Nayak, P. K.; Ramadan, A. J.; Wenger, B.; Lin, Y. H.; Snaith, H. J. Overcoming Zinc Oxide Interface Instability with a Methylammonium-Free Perovskite for High-Performance Solar Cells. *Adv. Funct. Mater.* **2019**, *29* (47), 1900466. https://doi.org/10.1002/adfm.201900466.

(14) Tang, C.; Shen, X.; Wu, X.; Zhong, Y.; Hu, J.; Lu, M.; Wu, Z.; Zhang, Y.; Yu, W. W.; Bai, X. Optimizing the Performance of Perovskite Nanocrystal LEDs Utilizing Cobalt Doping on a ZnO Electron Transport Layer. *J. Phys. Chem. Lett.* **2021**, *12*, 10112–10119. https://doi.org/10.1021/acs.jpclett.1c03060.

(15) Lee, Y.; Jeong, B. G.; Roh, H.; Roh, J.; Han, J.; Lee, D. C.; Bae, W. K.; Kim, J. Y.; Lee, C. Enhanced Lifetime and Efficiency of Red Quantum Dot Light-Emitting Diodes with Y-Doped ZnO Sol–Gel Electron-Transport Layers by Reducing Excess Electron Injection. *Adv. Quantum Technol.* **2018**, *1* (1), 1700006. https://doi.org/10.1002/qute.201700006.

(16) Wu, H.; Zhang, Y.; Zhang, X.; Lu, M.; Sun, C.; Zhang, T.; Yu, W. W. Enhanced Stability and Performance in Perovskite Nanocrystal Light-Emitting Devices Using a ZnMgO Interfacial Layer. *Adv. Opt. Mater.* **2017**, *5* (20), 1700377. https://doi.org/10.1002/adom.201700377.

(17) Dai, X.; Zhang, Z.; Jin, Y.; Niu, Y.; Cao, H.; Liang, X.; Chen, L.; Wang, J.; Peng, X. Solution-Processed, High-Performance Light-Emitting Diodes Based on Quantum Dots. *Nature* **2014**, *515* (7525), 96–99. https://doi.org/10.1038/nature13829.

(18) Fakharuddin, A.; Qiu, W.; Croes, G.; Devižis, A.; Gegevičius, R.; Vakhnin, A.; Rolin, C.; Genoe, J.; Gehlhaar, R.; Kadashchuk, A.; Gulbinas, V.; Heremans, P. Reduced Efficiency Roll-Off and Improved Stability of Mixed 2D/3D Perovskite Light Emitting Diodes by Balancing Charge Injection. *Adv. Funct. Mater.* **2019**, *29* (37), 1904101. https://doi.org/10.1002/adfm.201904101.

(19) Gunnarsson, W. B.; Rand, B. P. Electrically Driven Lasing in Metal Halide Perovskites: Challenges and Outlook. *APL Mater.* **2020**, *8* (3), 030902. https://doi.org/10.1063/1.5143265.

(20) Calloni, A.; Abate, A.; Bussetti, G.; Berti, G.; Yivlialin, R.; Ciccacci, F.; Duò, L. Stability of Organic Cations in Solution-Processed CH3NH3PbI3 Perovskites: Formation of Modified Surface Layers. *J. Phys. Chem. C* **2015**, *119* (37), 21329–21335. https://doi.org/10.1021/acs.jpcc.5b05422.

(21) Ng, Y. F.; Kulkarni, S. A.; Parida, S.; Jamaludin, N. F.; Yantara, N.; Bruno, A.; Soci, C.; Mhaisalkar, S.; Mathews, N. Highly Efficient Cs-Based Perovskite Light-Emitting Diodes Enabled by Energy Funnelling. *Chem. Commun.* **2017**, *53* (88), 12004–12007. https://doi.org/10.1039/c7cc06615e.

(22) Xing, J.; Zhao, Y.; Askerka, M.; Quan, L. N.; Gong, X.; Zhao, W.; Zhao, J.; Tan, H.; Long, G.; Gao, L.; Yang, Z.; Voznyy, O.; Tang, J.; Lu, Z. H.; Xiong, Q.; Sargent, E. H. Color-Stable Highly Luminescent Sky-Blue Perovskite Light-Emitting Diodes. *Nat. Commun.* **2018**, *9* (3541), 1–8. https://doi.org/10.1038/s41467-018-05909-8.

(23) Zhao, X.; Tan, Z. Large-Area near-Infrared Perovskite Light-Emitting Diodes. *Nat. Photonics* **2020**, *14*, 215–218. https://doi.org/10.1038/s41566-019-0559-3.

Table of Contents Figure: